Investigation of the Breakdown of Newtonian Gravity at Submicron Length-Scales

Christopher A. Gerig

Advisor: Professor J.C. Séamus Davis
May 20, 2011

Submitted to the
Department of Applied and Engineering Physics
of Cornell University
in Partial Fulfillment of the Requirements for the Degree of
Bachelor of Science with Honors

Abstract

We are studying the ultimate limits of force/position-sensing with nano-mechanical systems and SQUID-based classical accelerometers at extremely low temperatures, with a view towards developing new force-sensing tests for fundamental physics. Of immediate interest is a type of Cavendish experiment designed to detect gravity at micron-scale distances and measure departures from Newton's Law of Universal Gravitation in the nanometer range. An intermediate apparatus has been designed and built to oscillate a source mass evaporated onto a membrane, thereby inducing an oscillation (via gravity) of a test mass evaporated onto another membrane, which is separated from the former membrane by approximately 100 microns. These masses are screened from each other by a rigid superconducting shield to prevent electromagnetic cross-talk. The ultimate design has sufficient sensitivity to detect possible non-Newtonian forces at distance scales shorter than 1 micron.

Acknowledgements

First and foremost, I must thank my mentor and principal investigator, Séamus Davis. I first met him as my professor in 2008 for Honors Electrodynamics, and since day one he was extremely influential and shared my enthusiasm for physics. He always related everything to the forefront of research and placed much emphasis on the big achievements of previous generations, and also never held back on mathematical rigor and physics maturity. This continued into the following semester of 2008, where he taught my Honors Thermodynamics course. This course was supposed to be a basic introduction to "waves" and "classical thermo" with equal emphasis. He instead taught all of waves in one week, saying it was nothing but differential equations, and used the rest of the time to cover not only classical thermo, but statistical thermodynamics. Although most kids saw the material fly over their heads, I for once was not bored, took in all the material, and shared the same views that Séamus did on teaching. At that time I was looking to begin research, and he was the first (and only) professor I went to. At first he toured me around his lab, briefly mentioned the gravity experiment, and then tried to scare me away with the "realities of experimental physics research." I greatly appreciate the opportunity to work on this gravity experiment, and am honored to work under Séamus; best research opportunity ever.

Séamus left the research up to me, giving me infinite flexibility. I worked roughly from September 2008 to May 2011, some of which lacked efficient research progress due to a temporary loss of passion (a personal problem which has been resolved). Despite the inefficient progress, there has been much information learned and much work completed, and I owe thanks to the rest of the Davis group. Mo Hamidian wasn't afraid to pick on me when I was at a standstill in the research for a full week, and motivated me to demonstrate my competence. Along with Vikram Gadagkar, Sourin Mukhopadhyay, and Ming Chuang, they helped me overcome many obstacles of fundamental [experimental] research, especially cryogenic techniques. In particular, Ming was always patient and always available to guide me when hooking up the 4K-probe and cooling down the experiment. Ben Hunt (now a postdoc at MIT) took me under his wing during my first year in the group, providing me with the basics of detection techniques and the skills to build and test capacitive membranes. For this I thank him greatly.

Finally, to the undergraduate who came before me and obtained the grant to begin the gravity experiment, I thank Hiro Miyake (now a graduate student at MIT). The proposal [1] was selected for funding in the NIST Precision Measurement Grants program, and was awarded $\$150,000$. His overview of the experiment and initial calculations allowed me to develop and correct them further with great ease, ultimately bringing the experiment into realization.

Contents

1 Introduction

In a nutshell, our classical view of gravity is that it abides by the inverse-square law, i.e. that the gravitational force is inversely proportional to the square of the distance between two objects. However, String Theory's prediction of extra spatial dimensions creates a perturbation to this law, and this modified gravitational force now has an exponential decay dependence on distance (which becomes invisible at large enough separations). Our hope is to put a bound on the size and length scales where this perturbation could exist, or even to discover the perturbation and supply experimental evidence to String Theory.

1.1 Theoretical Motivation

1.1.1 QFT, GR, and Newtonian Gravity

What is *gravity*? Galileo Galilei (1564-1642) realized it as a force which accelerates any free-falling object at the same rate. This corrected the naive view of Aristotle, who thought larger objects fell with a larger acceleration. Isaac Newton then came along in 1687 with his *Principia*, a journal which defined the gravitational force as the following (translated from Latin): "Every particle of matter in the universe attracts every other particle with a force that is directly proportional to the product of the masses of the particles and inversely proportional to the square of the distance between them." In other words,

$$\overline{\mathbf{F}}_g = -\tfrac{GMm}{r^2}\hat{\mathbf{r}}$$

where $G \approx 6.67428 \times 10^{-11}\mathrm{m}^3\mathrm{kg}^{-1}\mathrm{s}^{-2}$ is the empirical gravitational constant (Figure 1). This is known as Newton's Law of Universal Gravitation. From this equation, three types of questions arise. In relation to G, how strong is gravitation? Is its value accurate, and is it always constant? In relation to M and m, does gravitation couple to mass and to mass only? Is the Equivalence Principle (inertial mass = gravitational mass) valid? And in relation to r, does the gravitational force drop like the inverse squared distance? This latter question is studied here.

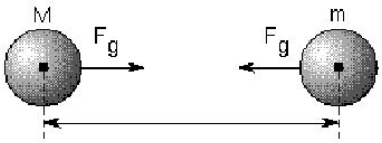

Figure 1: *Gravitational force between objects*

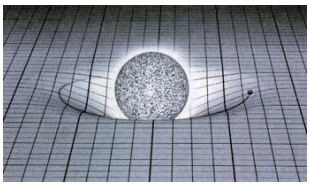

Figure 2: *Curvature of spacetime*

Rewriting the force as $\overline{\mathbf{F}}_g = m\overline{\mathbf{g}}$ where $\overline{\mathbf{g}}$ is the gravitational vector field, the inverse-square law can be recovered from Gauss' Law $\overline{\nabla} \cdot \overline{\mathbf{g}} = -4\pi G\rho$ where ρ is mass density. Defining the gravitational potential by $\overline{\mathbf{g}} = -\overline{\nabla}V$, this implies $\nabla^2 V = 0$ in a mass-free region, which in $\mathbb{R}^3$ corresponds to $F_g \propto \frac{1}{r^2}$.

This formulation in Classical Mechanics generalizes nicely into General Relativity, where instead of being viewed as a force, gravity is described by the warping of spacetime (Figure 2). Einstein's theory of GR is the unification of special relativity and Newton's Law, and it relates the presence of matter $T_{\mu v}$ to the curvature of space $G_{\mu v} \equiv R_{\mu v} - \frac{1}{2}Rg_{\mu v}$ via Einstein's field equations $G_{\mu v} + \Lambda g_{\mu v} = \frac{8\pi G}{c^4}T_{\mu v}$.

In addition to gravity there are three other fundamental forces. Listed from strongest to weakest, these four fundamental forces are the strong force, the electromagnetic force, the weak force, and the gravitational force. The strong force concerns binding in atoms. The electromagnetic force concerns charges and light, and the weak force concerns radioactivity and decay. With the exception of gravity, these three forces can be described as the quantum exchange of virtual bosons. In other words, Quantum Mechanics generalizes nicely using QFT (quantum field theories) to handle all of the fundamental forces *except* gravity. When we try to associate a QFT to gravity, i.e. we suppose gravitational interactions are mediated by 'gravitions', we encounter problems. While the quantized theory does extend to GR in the classical limit, it breaks down at the Planck-scale $M_P = \sqrt{\frac{\hbar c}{G}}$ (in particular, near the singularity of a black hole). But there are simpler disconnections between gravity and the other forces, namely, the Hierarchy Problem and the Cosmological Constant Problem (CCP).

The CCP arises from the evidence of Hubble that the expansion of the universe is accelerating, which can be explained by the *cosmological constant* $\Lambda = 8\pi\rho_{vac}$ appearing in Einstein's field equations. Here ρ_{vac} is the vacuum energy density. The problem is that certain theories predict $\Lambda = 0$, whereas other theories predict Λ to be on the order of M_P^4, and both of these claims disagree with the measured constant (of vacuum energy) which is on the order of $10^{-120}M_P^4$.

The Hierarchy Problem questions the huge strength difference $F_{weak}/F_g \sim 10^{32}$ between the weak scale and the gravity scale. As the electromagnetic force and weak force can be unified into the electroweak force, we may view this as the difference between two fundamental energy scales in nature, the electroweak-scale $M_{EW} \sim 10^{12}eV$ and the Planck-scale $M_P \sim 10^{27}eV$.

Further review of the history and problems of gravity can be found in [2].

1.1.2 String Theory and Non-Newtonian Forces

Obviously, a grand unified theory is needed to fundamentally connect QM to GR. One proponent is String Theory (or its extension M-Theory). String Theory asserts that the fundamental forces are "strings." The difference between gravity and the other three forces is that gravity is represented by a closed loop while the others are represented by open strings. The open strings are stuck to the universe like hair on our arms, but the closed string can propagate away from the universe, and interacts more on smaller scales where extra spatial dimensions are supposed to exist (hence appears weaker to us). Indeed, M-Theory asserts the existence of six compact spatial dimensions (in addition to our familiar

three dimensions), which are 6-dimensional Calabi-Yau manifolds present at every point in space. A good way to picture this is the following. Suppose you are walking on a suspended rope; you only have one direction of movement (back or forth). But if you shrunk yourself down to the size of an ant, you would see that at every point along the forward-backward dimension there is a second compact dimension, the diameter of the rope, that you can move around. As gravity interacts with these additional spatial dimensions, the Newtonian formulation is modified. In fact, theoretical explanations yield the Yukawa potential,

$$V = -\frac{GMm}{r}(1 + \alpha e^{-r/\lambda})$$

where the exponential decay term is a non-Newtonian perturbation. The behavior of gravity and the size of the extra dimensions are absorbed in the constants α (the characteristic strength) and λ (the characteristic length). So String Theory recasts the Hierarchy Problem into the question, "What is the size of these extra spatial dimensions?"

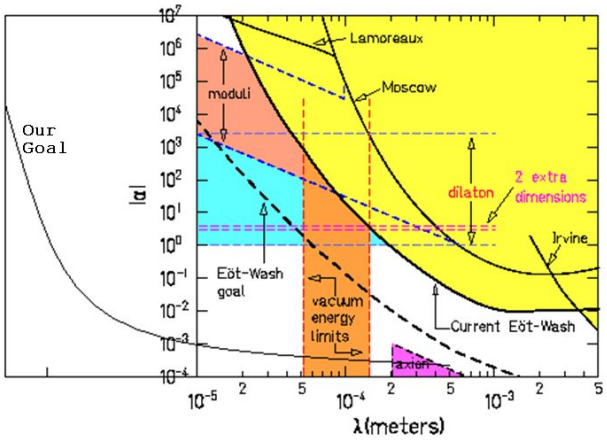

Figure 1: *(Un)explored regions of non-Newtonian effects*

In Figure 1 we see a plot of α against λ, where experimental observations have put bounds on these values (the yellow-shaded region indicates where the Yukawa term has been excluded). Also shown is our ultimate goal, the limit of where we plan to detect gravitational signals with our precision measurement techniques. As indicated in the other shaded regions, theories predict the existence of extra particles and physics that couple to the non-Newtonian force. As a byproduct we will confirm or destroy these hypotheses. For further information on the gravitational force and its Yukawa counterpart with String Theory, see [2].

1.2 Previous Experiments

In 1797, Henry Cavendish performed the famous and first experiment that measured the gravitational force between masses in a laboratory. Two small masses (balls) were attached to the ends of a thin rod that was suspended from a wire, and this lied between two large masses (Figure 1). The gravitational force between the masses would twist the rod by an angle θ until the torque-force on the wire matched the gravitational force. By calibrating the angles to the wire's torsion coefficient, F_g could be accurately determined. This experiment is equivalent to taking one mass, oscillating it, and detecting the induced oscillation in the other mass. Since then, there have been many experiments that mimic the Cavendish experiment, some of which will be briefly described here.

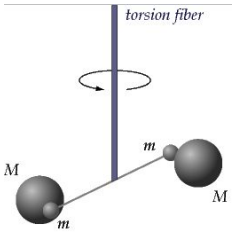

Figure 1: *Cavendish's torsion balance experiment*

In 2003, John Chiaverini of Stanford published his experimental work, which made use of a microcantilever [3]; see Figure 2. A mass attached to the cantilever was subjected to a time-varying gravitational force, namely that of a large mass a small distance away which was oscillated by a piezoelectric actuator. The cantiliver deflection was measured using fiber-optic interferometry and provided a measure of F_g. They achieved separation distances between the two masses around $25\mu m$.

In 2004-2007, Eric Adelberger and Charles Hoyle and Daniel Kapner of U. Washington published their experimental work, which made use of a torsion pendulum [4,5]; see Figure 3. They took a ring with holes and suspended it over a disk with holes. If the disk had no holes then gravity would pull down uniformly and no torque would occur. But the holes in the disk that are displaced from the holes in the ring create a Newtonian-torque, since gravity acts on the mass distribution. The pendulum twist was monitored using an autocollimator system. They achieved separation distances between the two masses from $10mm$ to $55\mu m$.

In 2008, David Weld of Stanford published his experimental work, which made use of a variable density mass and a microcantiliver [6]; see Figure 4. A disk with a varied density rotates under a test mass on a cantiliver, and so the induced gravitational force is time-varying. The mass displacement was measured with a laser interferometer, and the position of the drive mass was simultaneously recorded using an optical encoder. They achieved separation distances between the two masses around $30\mu m$.

In 2010, Ho Jung Paik of U. Maryland published his experimental work, which made use of two

oscillating membranes [7]. As their proposal is in essence the same as the one of this paper, we will not discuss it. They achieved separation distances between the two masses around $260\mu m$.

As of 2010, Stephan Schlamminger of U. Washington is doing a pendulum mass-distribution experiment; see Figure 5. The gravitational field of a homogenous infinite sheet of material is independent of position, $g(z) = 2\pi G\rho$. Therefore, if a pendulum is placed near the sheet and the pendulum has a mass distribution which is only displaced in the z-direction (orthogonal to sheet), then no torque is produced. In other words, torque can only be produced if there are non-Newtonian forces, such as the Yukawa force $g(z) = 2\pi G\rho(1 + \alpha e^{-z/\lambda})$.

As of 2010, researchers at NIST (Boulder, Colorado) have proposed an experiment where masses are separated by a few nanometers [8]; see Figure 6. A light beam will levitate a glass bead, and a large gold mass will oscillate near it to induce oscillations in the glass bead. No further information is known as of now (unless you give them a call).

Further information on previous experiments can be found in [3,9].

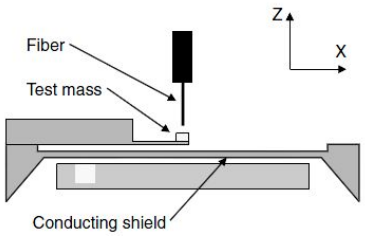

Figure 2: *Chiaverini*

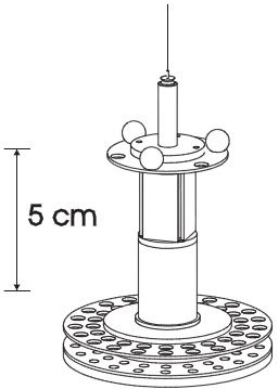

Figure 3: *Adelberger*

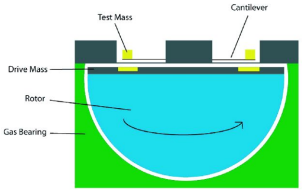

Figure 4: *Weld*

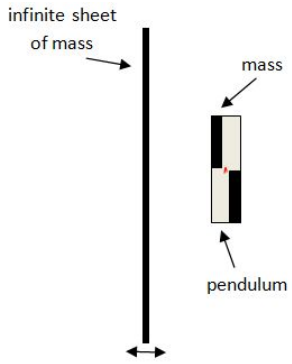

Figure 5: *Schlamminger*

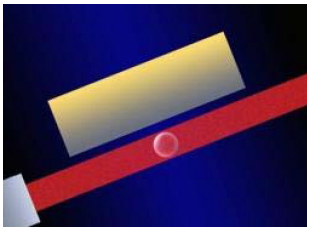

Figure 6: *NIST*

2 Our Proposal

The underlying concept of our experiment is the detection of a gravitationally induced oscillation of a test mass due to a driven oscillation of a nearby source mass. The apparatus will be suspended in a cryogenic vibration-isolation assembly, i.e. on an ultra low noise dilution refrigerator housed in an ultra low vibration and radio-frequency shielded laboratory. Both masses will be made of lead and will be evaporated onto respective membranes. Lead is very dense ($\rho_{Pb} = 11.34\text{g/cm}^3$) and is also superconducting, making it ideal for forming a large mass at low temperatures. One of the membranes will be Kapton and the other will be Silicon Nitride. Kapton HN (from DuPont) is very flexible and can be put under great tension, and retains its flexibility at low temperatures. Silicon Nitride (from Norcada or SPI Supplies) has a high quality factor at low temperatures, making it ideal for reacting to a gravitational pulse. Jack Harris determined its quality factor to be $Q \approx 10^7$ at $300mK$ [10]. It is important to localize the masses on the centers of the membranes. This reduces any change in tension and change in quality factor, and it reduces energy dissipation (lead is a lossy material).

2.1 Capacitive Membrane

In order to drive one of the masses (the source mass on the Kapton membrane) we make use of a coupling mechanism, microphonics. By evaporating a thin layer of gold ($\rho_{Au} = 19.30\text{g/cm}^3$) across the membrane and separating it from a fixed conducting plate, the membrane becomes a *capacitive membrane*, the top flexible electrode of a capacitor in a microelectromechanical system (MEMS); see Figure 1. The radius of the membrane is a, the radial direction is r, the vertical direction is z, the plate separation is d, the unit normal vector is $\hat{\mathbf{n}}$, and the membrane deflection is $z(r,t)$. We assume $d << a$ to not only get a large capacitance, but also to ignore fringing electric fields. From basic electromagnetism, the voltage between two plates held at a potential difference V_0 is given by $V = V_0(1 - \frac{z}{d})$, so that $\overline{\nabla} V = \frac{V_0}{d}\hat{\mathbf{n}}$. As the charge density on the plates is $\sigma = \varepsilon_0 |\overline{\nabla} V \cdot \hat{\mathbf{n}}|$ and the electric field due to the bottom plate is $\overline{\mathbf{E}} = \frac{\sigma}{2\varepsilon_0}\hat{\mathbf{n}}$, we obtain an attractive pressure on the top plate

$$P_e = \sigma E = \frac{\varepsilon_0 V_0^2}{2d^2} \ .$$

Therefore, by applying a voltage between the membrane and the bottom fixed electrode we can deflect the membrane due to the attractive electrostatic force.

Figure 1: *Capacitive membrane schematic*

It is important to know how the membrane behaves when a voltage is applied, noting that the electrostatic pressure (force) is nonlinear in separation distance d. For convenience we are assuming that P_e is uniform across the membrane – this really only occurs when the Kapton membrane is completely covered by the gold layer and is of the same diameter as the bottom fixed electrode. The damped driven wave equation is $T\nabla^2 z + P_e e^{i\omega t} = \mu\frac{\partial^2 z}{\partial t^2} + R\frac{\partial z}{\partial t}$, where μ is mass/area, T is tension/length, R is the damping coefficient, and $k = \omega/c = \omega/\sqrt{\frac{T}{\mu}}$. Due to our quality factor and dimensions, we can ignore damping (and R just gets absorbed into k anyway, $k^2 \mapsto \kappa^2 = \frac{\omega^2}{c^2} - i\frac{\omega R}{T}$). Using spherical coordinates the equation becomes $\frac{1}{r}\frac{d}{dr}[r\frac{dz}{dr}] + \frac{\varepsilon_0 V^2}{2T}\frac{1}{(d-z)^2} = 0$. We can linearize the driving force under small displacements z, with $\frac{1}{(d-z)^2} \approx \frac{1}{d^2}[1 + \frac{2}{d}z + \frac{3}{d^2}z^2 + \cdots]$, but calculations become messy. We instead assume that the distance in P_e is constant, and then the wave equation solution becomes $z(r,t) = \frac{P_e}{k^2 T}[\frac{J_0(kr)}{J_0(ka)} - 1]e^{i\omega t}$. The Bessel function $J_0(\chi)$ is approximated by $1 - 3\chi^2$ for $\chi < 1$, so that for $ka, kr << 1$ we get

$$z(r) \approx \frac{3P_e}{T}(a^2 - r^2) \ .$$

In other words, the vertical displacement of the membrane from equilibrium is a Bessel function, which under suitable approximations becomes a parabola.

The fundamental frequency for the circular Kapton membrane is $\omega_0 = 2.405c/a \approx 1$kHz, assuming $a = 5 \times 10^{-2}m$ and $T = \sigma_y t \approx 600\text{Pa} \cdot m$, where $\sigma_y \approx 60$MPa is the yield point stress (for permanent deformation) and $t \approx 10^{-5}m$ is the membrane thickness. The fundamental frequncy for the square SiN-membrane is $\omega_0 = \frac{\pi}{L}\sqrt{\frac{2\sigma_t}{\rho_{SiN}}} \approx 27$kHz, assuming density $\rho_{SiN} = 3\text{g/cm}^3$ and size $L = 5mm$ and tensile stress $\sigma_t = 250$MPa.

For more details on membrane deflections and microphonics, see [11,12,13].

2.2 Electrode Biasing

As shown above, we can apply an AC voltage to oscillate the capacitive membrane. But the electrostatic force exerted by a capacitor $F = \frac{CV^2}{2d}$ is not linear in the voltage. In order to make it linear (and amplify it), we apply a high DC voltage V_{dc} on top of the AC excitation $V_{ac}\cos(\omega t)$ with $V_{dc} >> V_{ac}$. Then

$$F \approx \frac{C}{2d}[V_{dc}^2 + V_{dc}V_{ac}\cos(\omega t)] = F_0 + \frac{CV_{dc}}{2d} \cdot V$$

where V is the AC excitation voltage and F_0 is the new equilibrium force. This constant equilibrium force simply puts a permanent deflection in the membrane, hence shifts the equilibrium spacing between the two masses. Therefore, electrode biasing can be used to feasibly manipulate the separation between masses, allowing us to probe and plot gravitational interactions.

2.3 Shielding

As any electromagnetic signals will overwhelm our expected gravity-signal, appropriate shielding must be used. The *Meissner Effect* states that superconductors expel magnetic fields. More precisely, a weak external magnetic field $\vec{H}$ penetrates the superconductor only a small distance $\lambda = \sqrt{\frac{m_e c^2}{4\pi n_s e^2}}$ (the *London penetration depth*), where n_s is the superfluid electron density; the magnetic field obeys the London equation $\nabla^2 \vec{H} = \frac{1}{\lambda^2}\vec{H}$. In particular, for a magnetic dipole moment $m\hat{z}$ brought near the entrance ($z = 0$) of an infinitely long superconducting cylinder of radius $r = r_0$, the magnetic field is given by $B_z(r, z) \approx \frac{3.83\mu_0 m}{2\pi r_0^3} \frac{J_0(3.83r/r_0)}{J_0(3.83)^2} e^{-3.83z/r_0}$ for $z >> 1$ [14]. Thus we should house our SiN-membrane in a tubular superconducting shield since magnetic fields are exponentially screened. Furthermore, between the two membranes there will be a thin superconducting sheet of Niobium (from Alfa Aesar) which deflects magnetic fields. Note that the Niobium thickness must be larger than the London depth $\lambda \approx 39nm$ as well as the *coherence length* $\xi \approx 38nm$ (the approximate spatial dimension of the Cooper pairs to form superconductivity).

This shielding does not take care of electrostatic fields, but grounding does. Our apparatus will act as a Faraday cage. And as the separation distances between membranes are greater than $100nm$, we can ignore Casimir forces and cross-talk.

2.4 Gravitational Force

2.4.1 Newtonian versus non-Newtonian

Recall that the Newtonian gravitational potential is $V_N = -\frac{GMm}{r}$ and the Yukawa potential is $V_Y = -\frac{GMm\alpha}{r} e^{-r/\lambda}$. For a point mass m separated from an infinite sheet of density ρ and thickness $2t$, the Newtonian force is $F_N = -4\pi G\rho t m$, independent of separation distance. So thanks to Gauss' Law we can ignore the membranes themselves in the gravitational force, and only the localized masses will have any contribution.

Consider a point mass m separated a distance z_0 away from the center of mass of a circular plate of density ρ, radius a, and thickness $2t$, with $a >> z_0 \sim t$. Then $V_N = -Gm \int_0^{2\pi} \int_0^a \int_{-t}^t \frac{\rho r\, dr\, d\theta\, dz}{\sqrt{(z_0-z)^2+r^2}}$, and hence the Newtonian force is $F_N = -\frac{dV_N}{dz}|_{z_0} \approx -4\pi G\rho t m(1 - \frac{z_0}{a})$. As for the Yukawa term $V_Y = -Gm\alpha \int_{-t}^t \int_0^a \int_0^{2\pi} \frac{\rho r\, dr\, d\theta\, dz}{\sqrt{(z_0-z)^2+r^2}} e^{-\frac{\sqrt{(z_0-z)^2+r^2}}{\lambda}}$ we can make the approximation $\sqrt{(z_0 - z)^2 + a^2} \approx a$ so that $V_Y = 2\pi Gm\rho\alpha\lambda \int_{-t}^t dz[e^{-\frac{\sqrt{(z_0-z)^2+a^2}}{\lambda}} - e^{(z-z_0)/\lambda}] \approx 4\pi Gm\rho\alpha\lambda[te^{-a/\lambda} - \lambda e^{-z_0/\lambda}\sinh\frac{t}{\lambda}]$. The Yukawa force is then $F_Y \approx 4\pi Gm\rho\alpha\lambda e^{-z_0/\lambda}\sinh\frac{t}{\lambda}$. Now consider the same scenario but extend the point mass m to a disk of radius $\epsilon << a$ and thickness δ, with separation distance h from the larger disk. Changing $m \mapsto dm = \pi\epsilon^2\rho_m\, dz_0 = \pi\epsilon^2 \frac{m}{\pi\epsilon^2\delta} dz_0 = \frac{m}{\delta} dz_0$ and integrating the two forces by $\int_{h+t}^{h+t+\delta} dz_0$, we obtain

$$|F_N| = 4\pi G\rho t m(1 - \tfrac{\delta}{2a} - \tfrac{h+t}{a}) \quad , \quad |F_Y| = 4\pi G m\rho\alpha\lambda^2 \tfrac{1}{\delta} e^{-\frac{h+t}{\lambda}}[1 - e^{-\frac{\delta}{\lambda}}]\sinh\tfrac{t}{\lambda} \ .$$

Setting these two values equal to each other will allow us to establish a bound on the α and λ values that we can observe.

2.4.2 Force Sensitivity

Assume that the source mass (coupled with the Kapton membrane) is an infinite sheet mass of surface density σ, and that the test mass is a point mass m with equilibrium separation x_0. The source mass is driven at $Ae^{-i\omega t}$, and the Yukawa force is $|F_Y| = 2\pi G\sigma m\alpha e^{-s/\lambda}$ where $s = x_0 + x + Ae^{-i\omega t}$ is the separation distance. We can take the force to linear order in s/λ, giving $|F_Y| \approx 2\pi G\sigma m\alpha e^{-x_0/\lambda}[1 - (x + Ae^{-i\omega t})/\lambda]$. The damped driven harmonic oscillator equation is then

$$m\ddot{x} + b\dot{x} + (k + 2\pi G\sigma m\alpha e^{-x_0/\lambda})x = -F_0 + 2\pi G\sigma m\tfrac{\alpha}{\lambda} e^{-x_0/\lambda} Ae^{-i\omega t} \ .$$

It has a periodic drive force, and we can ignore the constant term F_0 since it simply shifts the displacement $x(t)$. After approximating the damping coefficient $\gamma^2 = (k + 2\pi G\sigma m\frac{\alpha}{\lambda}e^{-x_0/\lambda})/mQ^2$ by $(\omega_0/Q)^2$, the amplitude at resonant frequency is given by

$$\delta x = \frac{2\pi G m A\sigma\alpha e^{-x_0/\lambda}/\lambda}{\sqrt{(2\pi G\sigma m\alpha e^{-x_0/\lambda}/\lambda)^2 + m^2\omega_0^4/Q^2}} \ .$$

Using expected values $\alpha = 1$, $\lambda = x_0 = 10^{-5}m$, $\sigma = 10^{-2}\text{kg}/m^2$, $A = 10^{-6}m$, $m = 10^{-7}\text{kg}$, $Q = 10^5$, and $\omega_0 = 1\text{kHz}$, the signal displacement is $\delta x \approx 10^{-14}m$. Using the SQUID-based detection scheme (discussed in Section 3.3.2), we should be able to resolve this signal above the noise.

3 Experimental Techniques

3.1 Cryogenics

We need an ultra low temperature environment to suppress intrinsic thermomechanical noise of the system that can overwhelm our signal. The equation of motion of a damped harmonic oscillator in a thermal bath is $m\ddot{x} = -kx - b\dot{x} + \sqrt{4k_BTb}$, with solution $x_{th} = \sqrt{\frac{4k_BTQ}{m\omega_0^3}}$ at resonant frequency [15]. Using expected parameters $m = 10^{-5}kg$, $Q = 10^5$, $\omega_0 = 10^3$Hz, we have that $x_{th} \approx (10^{-11}m) \cdot \sqrt{T}$ (per square-root hertz). Thus at $T = 10mK$ we can sufficiently suppress thermal noise ($x_{th} = 10^{-12}m/\sqrt{\text{Hz}}$) to resolve possible Yukawa-type displacements of $10^{-14}m$.

Our apparatus will be suspended in a cryogenic vibration isolation assembly on an ultralow noise dilution refrigerator (Figure 1). We will operate at a temperature of approximately $10mK$, at pressures below $10^{-7}torr$. Consequently, precautions must be taken when cooling from room temperature to $10mK$ because thermal cycling of materials can easily collapse the experiment. The components of our dilution refrigerator from the still and downward are from Janis Cryogenics. Minoru Yamashita designed the remainder, including the 1K pot and pumping lines and vacuum can. Two parallel charcoal nitrogen traps are placed next to the refrigerator and are used to filter out dirt that has gotten into the Helium-3 circulating through the refrigerator (the gas is absorbed into the charcoal pores).

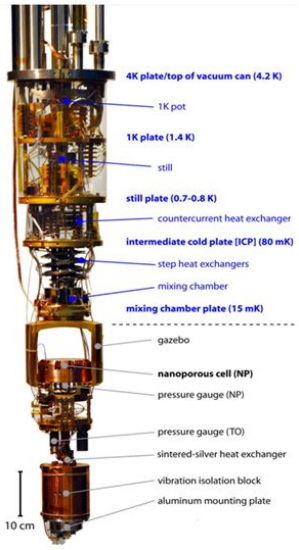

Figure 1: *Dilution Refrigerator*

Our dilution refrigerator reaches $4mK$ and is based on the separation of helium into two mixtures, the He3 rich-phase and the He4 rich-phase (both containing the other isotope). At low enough temperatures (obtained by submersing the refrigerator in liquid helium and using its 1K-pot), the He3 rich-phase becomes pure He3. But the He4 rich-phase goes to a constant He3 concentration of 6.6% (minimum). Thus by pumping He3 (using heat exchangers and the mixing chamber) from the poor-phase to the

rich-phase, the He3 from the rich-phase will flow to the poor-phase to restore equilibrium, and the latent heat of mixing (by crossing the phase boundary) cools the system down to an even lower temperature.

Reaching these near-absolute zero temperatures is necessary to make use of the properties of superconductors. The Meissner effect is used for magnetic shielding, and the zero-resistance effect is used for the helium-level indicator. The helium-level indicator is a superconducting rod with specified total resistance and length, and it measures how much liquid helium is in the dewar. When liquid helium rises up a certain length of the rod, that portion becomes superconducting and loses its resistance, thereby decreasing the total resistance of the rod and telling us the length of that portion.

As for thermometry, we can use either thermocouples or resistance thermometers. Thermocouples use the Seebeck effect to generate voltages, where two metals respond differently to a temperature difference. Resistance thermometers use the change in resistance due to changes in temperature. In particular, our apparatus uses a carbon reistor thermometer. As temperature rises, resistances rises, so we calibrate the resistances to the [Kelvin] temperatures (especially at room $300K$, nitrogen $77K$, and helium $4K$).

Further information on cooling and cryogenic equipment can be found in [16,17].

3.2 Vibration Isolation

We need an ultra low vibration environment to suppress background vibration noise that can overwhelm our signal. Our apparatus and dilution refrigerator will be housed in an ultralow vibration and radio-frequency shielded laboratory (Figure 1).

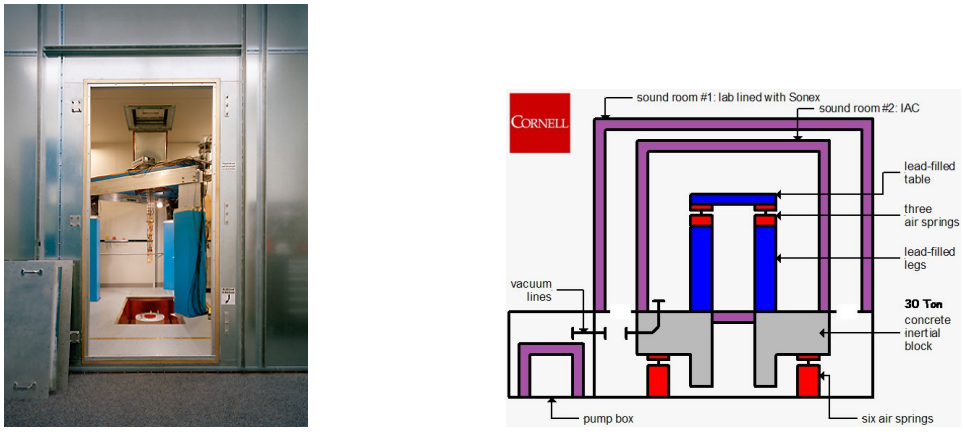

Figure 1: *RF shield room, and sound room suspension*

The RF (radio-frequency) shield room has a 30 ton foundation and suspended in an acoustically-shielded room via 6 air springs which serve as passive vibration isolators. Loaded into this room is a triangular table filled with lead, where the dilution refrigerator floats on it via 3 additional air springs.

This all exists in the basement of Clark Hall, and will be used for the final stage of our experiment. If we ever want further suppression, a 7-stage cryogenic vibration isolation system (cascaded spring-mass system) has been designed; detailed information is found in [18]. But it is not needed for our desired goal.

For immediate purposes, we simply make use of a small metal table floated on 3-air springs resting on the ground, which supports a large dewar. Of course, this will not be sufficient to resolve non-Newtonian signals, but it allows for more accurate readings of changes in capacitance. This crude vibration isolation system was demonstrated to suppress low-hertz noise by a factor of about one order of magnitude, using a geophone test. The *geophone* operates on the principle of electromagnetic induction, and converts ground displacements into voltage. It contains a suspended magnet surrounded by a coiled wire, so that external vibrations displace the magnet and hence generate a voltage (due to flux through the wire). Explicitly, for a coil with N turns, the voltage is $V = N\frac{d\Phi}{dt} = (N\frac{d\Phi}{dx})\dot{x}$.

Further information on vibration isolation can be found in [16].

3.3 Detection

Here we discuss the theory and utilization of a SQUID-based position sensor and a balanced Wheatstone capacitance bridge. Both are sensitive measurement devices which are very effective at low temperatures when vibrationally-isolated. We then briefly review how a lock-in amplifier works.

3.3.1 Wheatstone Capacitance Bridge

Once the capacitive membranes are built and assembled onto the apparatus, we must accurately determine their equilibrium capacitances and equilibrium separations from their respective fixed electrodes. To do this we use a balanced Wheatstone capacitance bridge (Figure 1), which is made up of a ratio transformer, a reference capacitor, and the experimental capacitor. The complete circuit also contains a lock-in amplifier, isolation transformer, DC bias voltage supply, and preamplifer. Our physical circuit uses an SR830 DSP Lock-in Amplifier, a Triad Magnetics SP-70 Isolation Transformer, an ESI DT-72A Dekatran Ratio Transformer, and an SR560 Low-Noise Preamplifier. The *ratio transformer* is a device which splits a variable inductor (of total inductance L) using a grounded "tap," giving two inductors with values $(1-\alpha)L$ and αL.

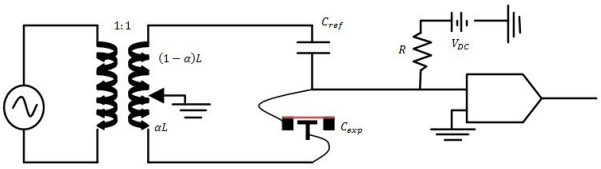

Figure 1: *Capacitance bridge circuit*

The main idea is that given a source voltage $E_0\cos(\omega t)$ and reference capacitance C_{ref}, we can "balance the bridge" by tuning α until $V_{out} = 0$. When this occurs (at α_b), the bridge is balanced and the experimental capacitance is given by

$$C_{exp} = (\tfrac{1}{\alpha_b} - 1)C_{ref}$$

We shall sketch a proof (using Figure 2):

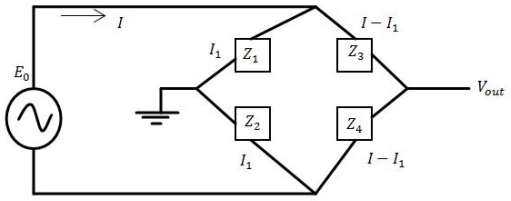

Figure 2: *Simplified bridge*

Here the impedances are $Z_1 = i\omega(1-\alpha)L$, $Z_2 = i\omega\alpha L$, $Z_3 = (i\omega C_{ref})^{-1}$, $Z_4 = (i\omega C_{exp})^{-1}$. Kirchhoff's law gives $E_0 = I_1(Z_1 + Z_2) = (I - I_1)(Z_3 + Z_4)$ and $V_{out} = I_1 Z_1 - (I - I_1)Z_3 = -I_1 Z_2 + (I - I_1)Z_4$. Solving for $V_{out} = E_0 \frac{(1-\alpha)C_{ref} - \alpha C_{exp}}{C_{ref} + C_{exp}}$, we get the desired relation between the capacitances at $V_{out} = 0$ (tuned $\alpha \to \alpha_b$).

As $C_{exp} = \frac{\varepsilon_0 A}{X}$, the equilibrium spacing in vacuum is

$$X = \tfrac{\alpha_b}{1-\alpha_b} \tfrac{\varepsilon_0 A}{C_{ref}}$$

Now when the capacitive membrane is displaced from equilibrium by $\triangle << X$, we have $C_{X+\triangle} = \frac{\varepsilon_0 A}{X(1+\frac{\triangle}{X})} \approx \frac{\varepsilon_0 A}{X}(1 - \frac{\triangle}{X}) = C_X + \delta C_X$, hence a perturbation $\delta C_X = -\frac{C_X \triangle}{X}$ (denoting the original experimental capacitance by C_X). This then perturbs the balanced α-value, giving $\alpha = \alpha_b + \delta\alpha$, and presents an off-balance AC output signal $V_B = \nu_\alpha \cdot \delta\alpha$. Here ν_α is a constant associated to α_b that can be determined directly by manually detuning α and recording V_B. The bridge equation gives $C_{X+\triangle} = (\frac{1}{\alpha_b + \delta\alpha} - 1)C_{ref} \approx C_X + \delta C_X \;\Rightarrow\; \delta C_X = -\frac{C_{ref} \cdot \delta\alpha}{\alpha_b^2}$. Putting this all together, the output is

$$V_B = \eta \cdot \triangle \;\text{ , where } \eta = \nu_\alpha C_{ref} \tfrac{(1-\alpha_b)^2}{\varepsilon_0 A}.$$

This provides a detection-scheme for measuring the oscillations of a capacitive membrane. The above description is unaltered when we add in stray capacitance C_s, except that it will shift the measured experimental capacitance. Care must also be taken to stabilize α and avoid drifting, and such is done by working at low temperatures and in a vibrationally-isolated room. The reference capacitor should be thermally coupled to liquid helium to help stabilization.

We lastly note how to obtain the spring constant K of the membrane. By applying a DC bias voltage V_{DC}, the experimental capacitance increases because the electrostatic pressure displaces the capacitive membrane towards the fixed electrode. Since $\frac{\delta C}{C_X}$ varies quadratically with the bias voltage $|V_{DC}|$, we

can step-up the bias voltage in discrete increments and fit the data to a straight line and extract its slope S. Equating the spring force to the electrostatic force, $\frac{C_X V^2}{2X} = k\triangle \approx k\frac{\delta C}{C_X}X$, we obtain

$$K \approx \frac{C_X^2}{2X^2 S}$$

There may be asymmetry when sweeping through negative to positive bias voltages, so one should obtain respective spring constants K_+ and K_- and take the average. A more accurate way to obtain K is explained in Appendix B of [19], giving $K \approx \frac{1}{2}\frac{\nu_\alpha}{\nu_V}\frac{C_X^2}{C_{ref}}\frac{\alpha_b^2}{X^2}(1 + 2 \cdot \ln\frac{A_d}{A_e})$. Here A_d is the full membrane area and A_e is the overlapping electrode area (of the evaporated material on the membrane), and the functional relationship $V_B = \nu_V V_{DC}^2$ allows us to extract ν_V.

For further information on the methods used with the capacitance bridge, see Appendix B of [19].

3.3.2 dc SQUID

A *Cooper pair* in a superconductor is a bound state of two electrons with opposite momenta and spins. They obey Bose-Einstein statistics, and the wavefunctions of the pairs overlap to a large degree. Consider cooper pair tunneling between two superconducting materials separated by a thin barrier (of cross-sectional area σ); this barrier is called a *Josephson junction*. The net current flowing through this junction contains a supercurrent component $I_S = I_C \sin\phi$ where $I_C = 2|K|n_s e\sigma/\hbar$ and $\phi = \phi_R - \phi_L$ represents the *Josephson phase* (difference in wavefunction-phases of the cooper pairs to the right/left of the junction); here K is a constant which depends on the characteristics of the junction. A chemical potential μ can result across the junction in the form of a potential difference V, giving $\mu = -2eV$. The Josephson phase is related to this potential difference via $\frac{\partial\phi}{\partial t} = -\frac{1}{\hbar}\mu = \frac{2e}{\hbar}V = \frac{2\pi}{\Phi_0}V$, where $\Phi_0 = \frac{h}{2e} \approx 2.07 \times 10^{-15} Wb$ is the flux quantum (a phenomenon associated with superconductors is magnetic flux quantization $\Phi \equiv \oint \vec{B} \cdot d\vec{a} = n\Phi_0$). The above tunneling process is called the *Josephson Effect*.

Superconducting Quantum Interference Devices (SQUIDs) are extremely sensitive magnetometers which make use of the Josephson effect and magnetic flux quantization. The *dc SQUID* consists of two Josephson junctions in parallel in a superconducting loop. It ultimately converts magnetic flux to a voltage, $V = \alpha\Phi$ where α is the *gain* of the device with units in volts per flux quantum. Further information can be found in [19,20,21].

There are two main techniques to use the dc SQUID as a position sensor, one depending on an oscillating magnet and the other depending on an oscillating superconducting surface. For completeness, both are described below.

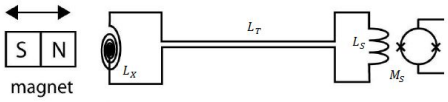

Figure 1: *Magnet SQUID sensor*

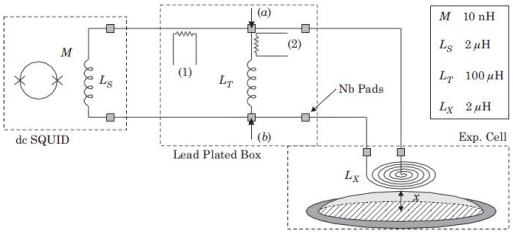

Figure 2: *SC-shield SQUID sensor*

The first position sensor is depicted in Figure 1 (the detection coil has turn density n_x and cross-sectional area σ). A magnet moves a distance δx relative to the detection coil. Such a displacement induces a change in flux at the detection coil, $\delta\Phi_x = \sigma\frac{\partial B}{\partial x}\delta x$. This causes an induced current I to preserve flux in the loop, $n_x\delta\Phi_x + (L_x + L_T + L_S)I = 0$. Via the mutual inductance M_S we obtain a flux change in the SQUID sensor, $\delta\Phi_S = M_S I = -M_S\frac{\sigma n_x}{L_x+L_T+L_S}\frac{\partial B}{\partial x}\delta x$. The SQUID converts this into a voltage, giving

$$\delta V = \eta \cdot \delta x \ \text{, where } \eta \equiv \frac{\delta V}{\delta x} = \alpha M_S \frac{\sigma n_x}{L_x+L_T+L_S}\frac{\partial B}{\partial x}$$

The second position sensor, which is the one we will be using in our experiment, is depicted in Figure 2 (the oscillating membrane is superconducting and is located a distance X away from the detection coil). Taking the whole circuit to be superconducting, the wires are heated up (they become non-superconducting) and currents I_x and I_S are injected into the wires. Then the heat source is removed so that the wires become superconducting; the currents are now trapped in the circuit. The importance of this is that through both circuit loops there can be no change in flux. Now the superconducting membrane moves a distance δx relative to the detection coil. The detection inductor has inductance $L_x = \mu_0 n_x^2 \sigma X$, so such a displacement induces a change in inductance $\delta L_x = \frac{L_x}{X}\delta x$. Since magnetic flux and inductance are related by $\Phi = LI$, a change in inductance δL_x induces a change in the current I_x in order to preserve the constant flux in the first loop, and this in turn induces a change in the current I_S, ultimately giving $\delta I_S = -I_x\frac{\delta L_x}{L_x(1+\frac{L_S}{L_x}+\frac{L_S}{L_T})}$. Via the mutual inductance M we obtain a flux change in the SQUID sensor, $\delta\Phi_S = M\cdot\delta I_S = -\frac{MI_x}{X}\frac{1}{(1+\frac{L_S}{L_x}+\frac{L_S}{L_T})}\delta x$. The SQUID converts this into a voltage, giving

$$\delta V = \eta \cdot \delta x \ \text{, where } \eta \equiv \frac{\delta V}{\delta x} = \frac{\alpha M I_x}{X}\frac{1}{(1+\frac{L_S}{L_x}+\frac{L_S}{L_T})}$$

The test membrane and the SQUID should be enclosed in a sealed niobium box for electromagnetic and flux shielding. The fundamental flux noise of our SQUID (from Quantum Designs company) is approximately $10\mu\Phi_0/\sqrt{\text{Hz}}$, and at one volt per flux quantum, with its sensitivity coefficient $\eta \equiv \frac{\delta V}{\delta x} \approx 1V/nm$, it inherits a background displacement noise of $x_{noise} \approx 10^{-14}m/\sqrt{\text{Hz}}$. But in our lab we actually obtain a resolution of $10^{-16}m/\sqrt{\text{Hz}}$ at $20mK$ [22].

For further information on the methods used with the SQUID, including construction, see Appendix A of [19] and Section 2.2.2 of [23].

3.3.3 Lock-in Amplifier

A lock-in amplifier can extract a signal which is modulated due to a noisy environment. It cleans the signal by using a reference signal and a low-pass filter.

Let $\tilde{V}_s = V_s \sin(\omega_s t + \theta_s)$ be the input signal $\tilde{V}_r = V_r \sin(\omega_r t + \theta_r)$ be the amplifier's reference signal. Both signals are multiplied to get an amplified signal $V_0 = \tilde{V}_s \tilde{V}_r = \frac{1}{2} V_s V_r [\cos(\triangle_\omega \cdot t + \triangle_\theta) - \cos(\omega_0 t + \theta_0)]$, where $\triangle_\omega = \omega_s - \omega_r$ and $\omega_0 = \omega_s + \omega_r$ (similarly for $\triangle_\theta$ and θ_0). AC signals are then removed via a low-pass filter. If $\triangle_\omega = 0$ then $V_0 = \frac{1}{2} V_s V_r \cos(\triangle_\theta)$, and if $\triangle_\omega \neq 0$ then $V_0 = 0$. The above process is then repeated using $\tilde{V}_s$ and a new reference $\tilde{V}_r e^{-i\pi/2}$, which gives an amplified signal $V_1 = \frac{1}{2} V_s V_r \sin(\triangle_\theta)$. The magnitude of the signal vector is taken to get rid of the phase-dependency, $R = \sqrt{V_0^2 + V_1^2} = \frac{1}{2} V_s V_r$, and this is then calibrated to obtain the output V_s.

The lock-in works by sweeping through ω_r-values until $\triangle_\omega = 0$ (giving output V_s), noting that when this frequency-difference is nonzero the output is zero.

3.4 Procedures

3.4.1 Cleaning

It is obviously important to clean all of the materials you handle. Dirt and even dust particles can easily destroy spacing between membranes and break vacuum seals. And once the apparatus is being pumped on to reach vacuum, those dirt particles will present a virtual leak that will show up on the leak detector.

The general procedure for cleaning an object is to first submerse it in acetone in a beaker and place it in the sonicator (for approximately 5-10 minutes). Once that is done, wash it with IPA (isopropyl alcohol). It is ideal to do this procedure without any stycast on the object, because the acetone will eat away at it. But as long as the acetone is on the stycast for a small period of time and you rinse it off, there is no problem. But for a more extensive cleaning process for objects that have stycast on them, skip the acetone and wash it with soapy water, and then with just water, and then with IPA.

Once the pieces are assembled together or the membranes are glued onto the pieces, you should simply use a swab with a little acetone (and then IPA).

For drying, letting the pieces just air-dry and wiping them with Kimwipes suffices.

3.4.2 Epoxy, Stycast

Epoxy is a copolymer, a "glue" that results from the mixture of two components (the resin and hardener). Except for the silver epoxy, this is used as an insulator to separate metals from each other, and is used to attach membranes to their rings. For temporary gluing purposes, or for objects that won't be placed in vacuum and cold temperatures, the cheap five-minute epoxy works great.

Stycast is a type of epoxy of high quality that works under many conditions. There are the two components, partA and partB, that are mixed at a certain ratio and cured over a specified time interval. This time interval can be decreased if you cure the stycast at a higher temperature, and you should check the stycast's data sheet for further information. The procedure for making stycast requires two weighing trays, a syringe, a small wooden stick, and a small rod. Use the wooden stick to pour some partA into a weighing tray, and weight it (x grams, aim for $x \gtrsim 1g$). Then pour some partB into another weighing tray, and use the syringe to drop partB into partA until the total weight is $x(1+m)$, *where m is the mix ratio of partB-to-partA*. Finally, mix the stycast using the rod for approximately 10 minutes, and let it cure (harden) for the appropriate amount of time (as found on the stycast's data sheet).

Silver epoxy is an electrically conductive silver-filled epoxy for connections which cannot be soldered. For the silver epoxy in our lab, the mix ratio is 1 : 1.

STYCAST 1266 (from Emerson & Cuming) is a clear, low viscosity encapsulant which, when fully cured, has outstanding toughness and impact strength. Its mix ratio is 28 : 100.

STYCAST 2850 GT (from Emerson & Cuming) is a two component, thermally conductive epoxy encapsulant that is used with Catalyst 24LV (partB). It features a low coefficient of thermal expansion and excellent electrical insulative properties. Its appearance is black, and its mix ratio is 7 : 100. This stycast cannot really be machined (it will break your drill-bits) and is only casted. The great advantage to its use is that it has an almost identical thermal expansion coefficient to that of brass, which is important when thermal cycling of the apparatus occurs.

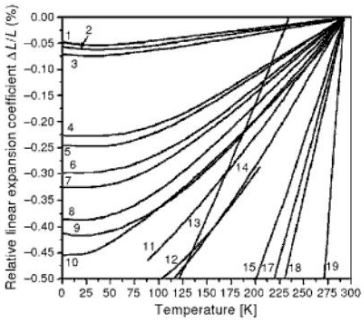

Figure 1: *Thermal expansion rates, 8 = Brass, 9 = Stycast 2850GT*

3.4.3 Vacuum Seal

We make use of indium in the form of an O-ring to create a vacuum seal between the 4K-plate and the vacuum can. The procedure is to first clean both surfaces. Be gentle and place indium wire around the vacuum can to form the ring at the right size. Apply a small amount of vacuum grease to the indium and place it back on the vacuum can. Push the two ends of the indium wire together to form the ring. Try to get a uniform thickness at the joint, which is helped by cutting a diagonal on both ends. Ultimately, the indium seal is very forgiving, so the joint and the tightness around the vacuum can need not be perfect. But do check for hair strands and other particles that might get on the indium O-ring and hence destroy the seal. When attaching the vacuum can to the 4K-plate, apply even pressure so that the indium seal deforms uniformly and does not break.

3.4.4 Leak Checks

Leak checks must be done to ensure that the vacuum seal, welding/soldering joints, and O-rings between tubing are not damaged. Any leak will not only stop you from reaching high vacuum (low pressures), but it can allow water to condense on the apparatus. The leak test procedure uses the diaphragm and turbo pumps, the leak detector, and a helium-spray.

Make sure all valves on your system and pumps are closed. First turn on the diaphragm pump; this is a rough pump which handles higher pressures. Then turn on the turbo pump; this is a more sensitive pump which uses thin blades at high speeds and gets you down to low enough pressures. Then open the valve between the two pumps, and open the valve to the rest of the system/apparatus. At low enough pressures, close the valve between the pumps, turn on the leak detector, and turn off the diaphragm pump. Replace the diaphragm pump with the leak detector and start pumping with the leak detector. Next, stop the detector pump, open the valve between the pumps, and restart the detector pump. This is a safety measure to not damage the detector pump.

We now use a spray-nozzle hooked up to a helium gas bottle. Try to localize where the helium gas flows, which might require "bagging" certain parts of the system. Spray the gas in short bursts. Check every possible joint. If there is a leak, the gas will enter the system and be picked up by the leak detector. Any [repeatable] increase in the helium leak rate above the background level is a problem.

To end the procedure, stop the detector pump, close the valve between the pumps, vent the detector, and shut off both pumps. Close off the valve to the system so that the apparatus remains in vacuum.

Note that helium-4 gas will leak through the fiber neck glass of the dewar, so there will no longer be vacuum in the dewar jacket. Thus the dewar jacket needs to be pumped out every month or so.

4 Construction and Progress

Although the ultimate design of the experiment involves one capacitive membrane (with microphonics for driving oscillations) and one SiN membrane (with SQUID-based detection), an intermediate experiment will simply replace the SiN membrane with another copy of the capacitive membrane of smaller size. Instead of the SQUID-based detection scheme, the Wheatstone capacitance bridge would be used to detect changes in capacitance (hence membrane displacements), as explained in Section 3.3.1. This simultaneously tests half of the apparatus from the ultimate design, and attempts to detect Newtonian gravity. The schematic of this intermediate apparatus is depicted in Figure 1, alongside its realization (red lines are capacitive membranes and blue line is Niobium shield). Each part was designed using SolidWorks, a CAD-software, and then sent to the machinists at Cornell to be built.

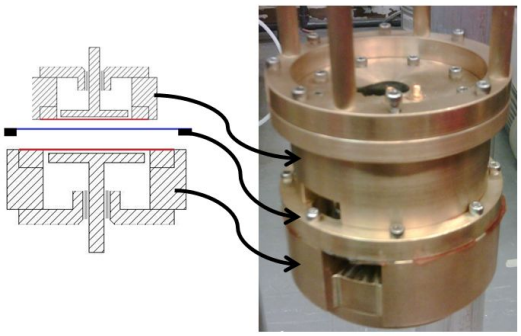

Figure 1: *Intermediate apparatus*

4.1 Assembling Capacitors

The capacitor in our apparatus has five main parts: the base, the bottom plate, the rigid capacitor plate, and the capacitive membrane ring (Figure 1). The rigid capacitor plate is specified to be flat within $25\mu m$. All pieces are cleaned before being assembled. The size of this capacitor is as large as it can be, because it must fit inside the vacuum can (diameter $4.5in$) and ultimately fit onto the dilution refrigerator (determined by still shield diameter $4.5in$).

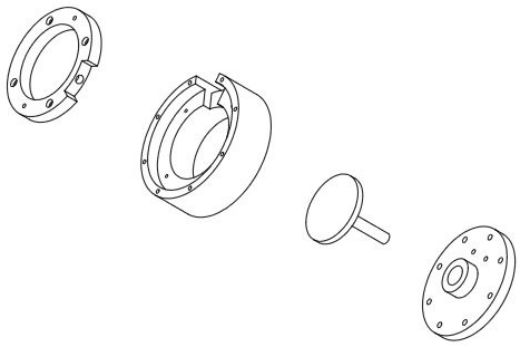

Figure 1: *Larger capacitor*

The Kapton membrane is put onto the membrane ring via a 2-stage process. In addition to the membrane ring there is a larger ring that circumvents the membrane ring. A little bit of 5-minute epoxy is poured along the larger ring, and is placed face down on top of a piece of Kapton film ($50\mu m$) on a flat surface. Once the glue dries, a little bit of Stycast 1266 is poured along the membrane ring and the larger ring slides over the membrane ring, acting as a weight to put tension on the Kapton film along the membrane ring (it uniformly stretches over the ring). Once this epoxy cures (10 hours at room temperature), the Kapton film is trimmed along the membrane ring.

To put a layer of gold onto this membrane, a mask is screwed onto the ring (Figure 2). The mask is a cutout of a circular electrode and a tab, and it can swivel on the membrane ring before it is screwed down in order to freely orient the tab. This tab is used for wire-connections to the membrane. The mask-ring object is then brought to the CCMR facility at Cornell, where it is placed in a vacuum chamber and has gold evaporated onto it. The total thickness of the gold layer is approximately $1\mu m$, and the deposition rate is $.5\mathring{A}/s$ (it should be this slow in order for the gold to be layered uniformly and for the membrane to not become damaged by the heat flow).

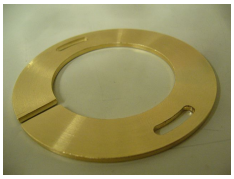

Figure 2: *Mask*

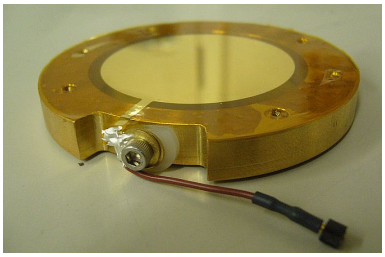

Figure 3: *Capacitive membrane with wire-connection*

On the side of the membrane-ring there is a small cutout with a clearance hole. Stycast 1266 fills the hole, cures, and is then tapped (i.e. threads are drilled through) for a heli-coil to be inserted. This allows a bolt to screw into the side of the ring, while being insulated from the ring. To establish a wire-connection to the membrane, the gold tab is bent and clamped between two brass washers, and this collection is screwed into the side hole of the ring with a teflon washer between the first brass washer and the side of the ring. One of the brass washers has a wire with a Samtec female connecter soldered onto it. The capacitive membrane is then complete (Figure 3).

In order to create the capacitor with a specified spacing between the plates, the base and bottom plate must be used as place holders. The capacitive membrane is screwed into the base and then layed upside down with the membrane touching an extremely flat surface. A piece of Kapton film of thickness $100\mu m$ then lies on top of the membrane and the rigid capacitor plate lies on top of that – the piece of Kapton film is a spacer which will give the permanent separation between the rigid capacitor plate

and the capacitive membrane. The bottom plate is then screwed onto the base, and the bottom plate has a hole in its center for the shaft of the rigid capacitor plate to go through. Stycast 2850GT is then poured in that center hole of the bottom plate which bonds to the shaft of the rigid capacitor plate. In order for the stycast to not pour down onto the capacitor plate itself, a small piece of plastic originally covers the hole of the bottom plate and is then punctured for the rigid capacitor plate to slide through (the plastic then acts as a back panel to stop the flow of stycast). It is important to place a weight on top of the shaft of the rigid capacitor plate so that the stycast doesn't pull the capacitor plate up while it contracts due to curing. After the curing is finished, the bottom plate (which is now bonded to the rigid capacitor plate) is taken off of the base, the spacer is removed, and then the bottom plate is screwed back in. There is now a $100\mu m$ spacing (approximately) between the rigid capacitor plate and the capacitive membrane.

Two microdot bulkhead jacks (from Tyco Electronics) were placed on the bottom plate, one being used for electrical connection to the bottom capacitor plate, and the other used for electrical connection to the capacitive membrane (Figure 4+5). The Samtec female connector on the capacitive membrane connects into a Samtec male connector which is directly attached to the microdot, and this allows the membrane to be disconnected at any point and replaced with another one.

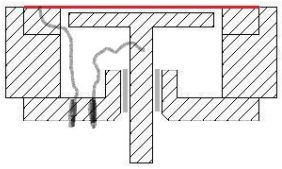

Figure 4: *Wire schematic of capacitor*

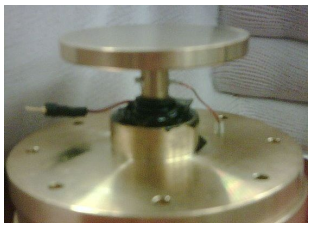

Figure 5: *Wire connections on bottom plate*

The above setups implicitly referred to the larger capacitor. The smaller capacitor has the same assembly as the larger capacitor, except that the membrane ring is small enough for a Nb-shield ring to fully slide over it (Figure 1). The Nb-shield has a thickness $40\mu m$. Annuli cut out from Kapton film are the spacers that separate the membranes from the Nb-shield, and holes are appropriately made in the annuli so that screws may pass through when screwing the apparatus together.

The tab the is bent and clamped between washers will always have a "bump" that extends off the plane of the membrane, and this can touch the Nb-shield when the apparatus is assembled. To remedy this, place a small piece of Kapton film over the bump so that the Nb-shield will not short to it.

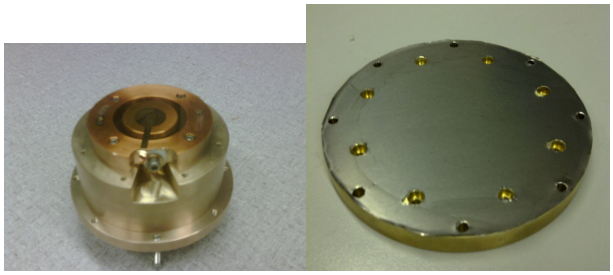

Figure 1: *Smaller capacitor and the Niobium shield*

4.2 The 4K-Probe

In order to test the apparatus, a dip probe needed to be built which would submerse the apparatus (inside a vacuum can) in liquid helium in a specific dewar, allowing the system to reach a temperature of $4K$. This probe consists of a $300K$ plate at the top where all wires/connections begin, a $4K$ plate at the bottom where the vacuum can latches onto and where the SQUID rests, and six radiation shields for obvious purposes (Figure 1). There is a central tube for wires and it is simultaneously the pump line for the vacuum can. Another tube with a bent neck has a set of wires. There is a tube for pouring in liquid nitrogen and liquid helium with a transfer stick, and there is a gas port for pressurization purposes, and there is another open port for the helium level indicator. On the $4K$ plate there are "feedthru" towers which can be transformed at a later point to house certain objects, and they provide better thermal contact due to increased surface area. There is also the *cold finger*, a piece of copper that thermally links the outside of the vacuum can to the inside, ensuring that the apparatus stabilizes at liquid helium temperatures; a braided copper strand hooks onto the cold finger and the apparatus to provide direct contact (visible in Figure 2, wrapped around the brass rod).

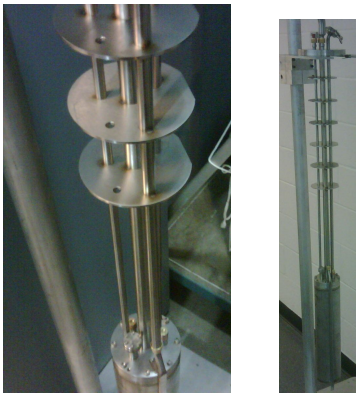

Figure 1: *4K dip probe*

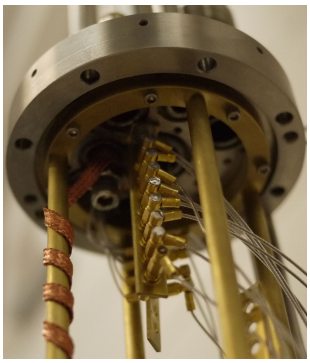

Figure 2: *Microdot junction and coax-wiring*

The wires on the probe are cryogenic coaxial cables (type SS, from Lake Shore). They terminate at the top of the probe at BNC jacks, where they are only connected at the pin (the outer shield of the

cable is left in suspension). They terminate at the bottom of the probe at microdot bulkhead jacks that are thermally linked and secured onto two junctions (Figure 2). The process for soldering coax wires to microdots is tedious – the instructions are found on the Tyco website. The apparatus then suspends from the $4K$ plate via a "gazebo" (four suspension rods) and hooks up to the microdot junction via coax wires whose ends are microdot angle plugs (Figure 3). All of the wires should run close to conducting ground plates (i.e. the walls of the tubes) in order to reduce fringing electric fields.

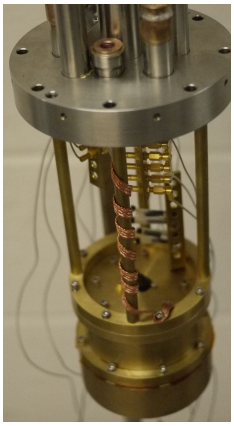

Figure 3: *Apparatus on probe*

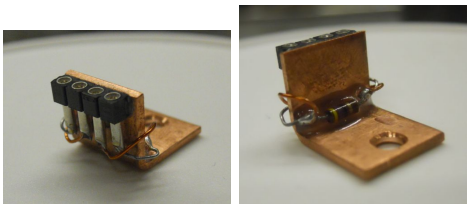

Figure 4: *Resistor thermometer*

Figure 4 shows the carbon resistor that acts as our thermometer. It screws onto the bottom of our apparatus, and uses a 4-point resistance measurement. Instead of microdots, this thermometer is connected by four Samtec connectors. As for calibration, at $300K$ the resistance is 49Ω, at $77K$ the resistance is 58Ω, and at $4K$ the resistance is 252Ω.

The wire connections are labelled at the top of the probe by integers $1-8$ and A, B, C, D (the latter ones are used for the 4-point thermometer). They way they connect down at the microdot junctions are as follows. The junction that has eight microdots reads $1-8$ as you move away from the $4K$ plate, and the other junction reads D, B, C, A. Anyone can change the ordering around if they want to unscrew and switch the microdot locations.

Every time this probe is used, the resistances of the wires should be checked to make sure they are at least in the $G\Omega$-range (otherwise there are probably slight shorts at the microdot/BNC terminals). Leak tests must be carefully run on the $4K$ plate, since there are soft solder joints, weld joints, braze joints, and vacuum seals that may have become cracked from the previous cool down. The O-rings that connect tubes together (i.e. the pieces at the top of the probe which connect to the pump) must be cleaned with IPA and should not be touched by bare hands; a little vacuum grease should be put on them before they are placed between the tubes.

4.3 Capacitor Tests

The capacitor is made up of a rigid capacitor plate and a capacitive membrane. Since the actual electrode is the gold layer, the Kapton membrane is a dielectric spacing (with permittivity $\sim 3.5\varepsilon_0$). The capacitance is thus $C = \frac{C_{Kapton}C_{space}}{C_{Kapton}+C_{space}} \approx \frac{\varepsilon_0 \pi r^2}{d_s + \frac{2}{7}d_K}$, where r is the radius of the smaller circular electrode and d_K is the thickness of the Kapton membrane and d_s is the spacing between the membrane and rigid capacitor plate. The [first] tests on the larger capacitor were done using just the vacuum can and a $4K$ flange (Figure 1), along with a makeshift styrofoam dewar to hold liquid nitrogen.

Figure 1: *Vacuum can and 4K flange*

All tests have only been performed on the larger capacitor. The first test was to measure the experimental capacitance at both $300K$ and $77K$, in vacuum, using the Wheatstone capacitance bridge (the input voltage was $200mV$ and the frequency was 1.8kHz). Because the reference capacitor was slightly unstable and there were drifts in the capacitance, many measurements had to be taken over a relatively long time period. The experimental capacitance (in air) was $C_{exp} \approx 445pF$ and so the spacing of the capacitor was $x_{eq} \approx 75\mu m$. Under these conditions the capacitor successfully passed the DC Bias Test. A biased DC voltage was applied to the capacitor in increments of $1V$, sweeping from $-10V$ to $+10V$, and the capacitance was measured at each increment (Figures 2+3). The signal-to-noise (standard deviation divided by mean) had a high resolution of $.23ppm$, but there was some assymetry in the capacitance plots when the bias voltage was swept across its range (and the base value of capacitance occurred at a bias voltage of $-1V$ instead of $0V$). This difference between the positive and negative bias is explained by a charge stuck on the apparatus, so that charge must be accounted for and calibrated out of the signal. The plots agree with the fact that $\frac{\delta C}{C}$ varies quadratically with the bias voltage $|V_{DC}|$. From this the spring constant of the membrane was determined to be $K_+ \approx 1051N/m$ and $K_- \approx 1371N/m$ for positive and negative biases, respectively. When this test was repeated at $77K$, the spring constants changed to $K_+ \approx 459N/m$ and $K_- \approx 714N/m$, approximately half that of the spring constants determined at $300K$. The reason for this is that when placed in liquid nitrogen, the thermal cycling of the brass weakened the tension it provided on the membrane, so that the spring constant was permanently decreased. A subsequent test at $300K$ agrees with the $77K$ results.

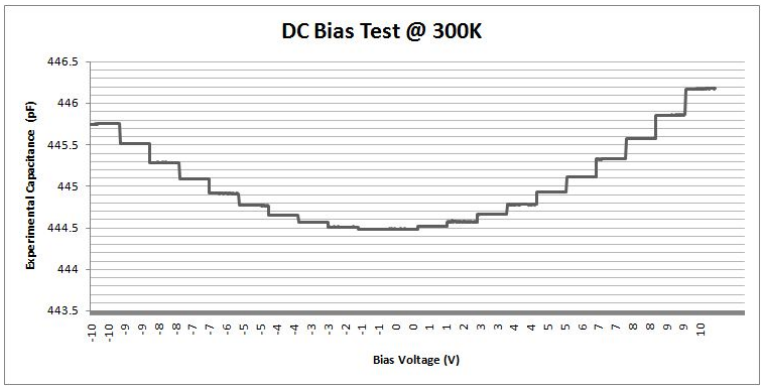

Figure 2

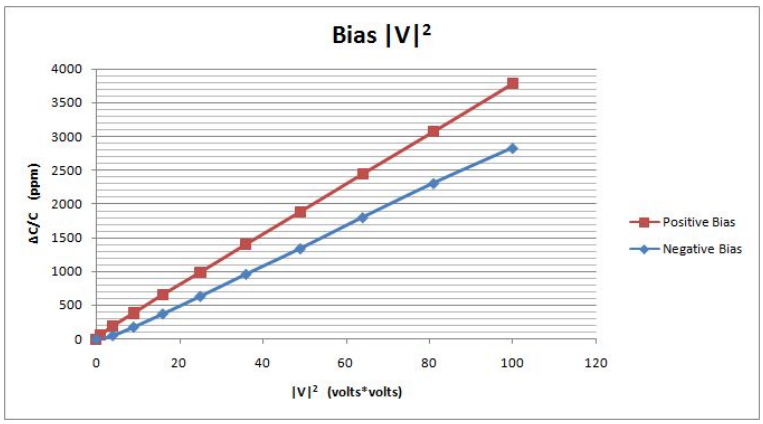

Figure 3

As of May 2011, with the apparatus assembled, the capacitance of the smaller capacitor is $27pF$ and the capacitance of the larger capacitor is $498pF$. The stray capacitances of the coax wires were measured to be $100pF - 150pF$. By using an aero-duster to blow some air on the membranes, the membranes deflect, so the membranes are not touching their respective rigid capacitor plates. But when cooled down to $77K$, the membranes did collapse onto the Niobium shield. Subsequently, additional spacers have been added between the shield and membranes, and the Niobium shield was replaced (there were visible dents on the original shield, which would destroy the spacings).

5 Future Plans

The immediate next step of the gravity research is to run the DC Bias tests on both capacitors at $4K$ and ensuring that the membranes do not collapse onto the Nb-shield. We will then proceed to running the Cavendish-experiment, where we oscillate the source mass and try to detect Newtonian oscillations in the test mass via the capacitance bridge technique. For the initial tests the gold layer can act as the mass, but ultimately we will evaporate a localized piece of lead onto both membranes.

There are some design modifications that will be of use in the future. The central hole in the bottom apparatus plate (which holds the shaft of the rigid capacitor plate) should be made smaller, so that less Stycast 2850GT is needed to pour. All wires should be cryogenic coax, and all connections should be microdot connections (instead of Samtec connectors). Instead of having the membrane ring of the larger capacitor rest inside the base of the apparatus on that lip, the lip should just be removed and the membrane ring should be made wider to extend across the whole top of the base – otherwise the two surfaces (lip of base and the ring) will easily be unlevel with respect to each other, and this is bad for achieving micron-scale spacing. The reference capacitors should be enclosed in a copper box (filled with stycast) with microdot connection ports. As for the Niobium shield, we can do better than $40\mu m$ by using perhaps a $5\mu m$ SiN-film and evaporating $100nm$ of Niobium onto both sides.

The protoype for the apparatus using the SiN-membrane is shown in Figure 1. The SiN-membrane is not circular but square with a square frame, and this will be attached to piece-3. Piece-4 is a tubular Niobium shield, and piece-5 is the ring for the Niobium film shield.

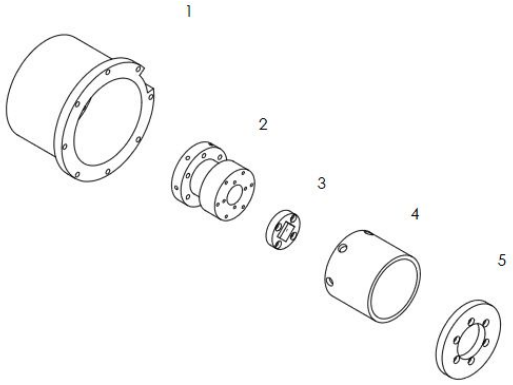

Figure 1: *Protype design of SiN-membrane part of apparatus*

There are also potential problems to consider, minus the obvious force sensitivity isssues (vibration isolation and signal-to-noise). Misalignments of the capacitors will alter the gravitational signals, giving inaccuracy on the α, λ values. We should thus design/use a capacitive position sensor to measure the relative tilt of the masses. Effects of thermal cycling must be considered; it weakens membrane tension and can alter the deflection and separation of the membranes (all of these have occurred). Thus we must

ensure appropriate spacing between capacitor plates and between membranes.

There will always be stray capacitance, and this gives inaccuracy of the experimental capacitances and hence displacements. These stray capacitances must be known in order to calibrate them out of the desired signals. Other stray capacitances should be located and suppressed, because they present noise to the signals via capacitive couplig. In particular, for a device with total impedance Z, an incoming signal $V(t)$ will have a noise $V_{noise} \sim V(t)\frac{Z}{Z+\frac{1}{j\omega C_{stray}}}$, where the stray capacitance is a capacitor that is in series with the device impedance.

6 Bibliography

[**1**] H. Miyake, *Precision Measurement of Gravitational Forces at the Submicron Length Scale*, (2007).

[**2**] E. Adelberger et al., *Tests of the Gravitational Inverse-Square Law*, Annu. Rev. Nucl. Part. Sci. 53 (2003).

[**3**] J. Chiaverini et al., *New Experimental Constraints on Non-Newtonian Forces below* $100\mu m$, Phys. Rev. Let. 90 (2003).

[**4**] C. Hoyle et al., *Submillimeter Tests of the Gravitational Inverse-Square Law*, Phys. Rev. D70 (2004).

[**5**] D. Kapner et al., *Tests of the Gravitational Inverse-Square Law below the Dark-Energy Length Scale*, Phys. Rev. Let. 98 (2007).

[**6**] D. Weld et al., *New Apparatus for Detecting Micron-scale Deviations from Newtonian Gravity*, Phys. Rev. D77 (2008).

[**7**] H. Paik et al., *Cryogenic Test of the Gravitational Inverse-Square Law*, WSPC Proceedings (2010).

[**8**] Web article, *Gravity Up Close: Looking for Extra Dimensions by Measuring Gravity at the Microscopic Level*, www.physorg.com (2010).

[**9**] D. Kapner, *A Short-Range Test of Newton's Gravitational Inverse-Square Law*, thesis (2005).

[**10**] B. Zwickl et al., *High Quality Mechanical and Optical Properties of Commercial Silicon Nitride Membranes*, arXiv:0711.2263 (2007).

[**11**] D. Raichel, *The Science and Applications of Acoustics* – Chapter 6, Springer (2000).

[**12**] J. Pelesko & D. Bernstein, *Modeling MEMS and NEMS*, CRC Press (2003).

[**13**] J. Warren et al., *Capacitance-Microphone Static Membrane Deflections*, Acoustical Society of America (1972).

[**14**] Y. Levin & F. Rizzato, *Superconducting Pipes and Levitating Magnets*, Phys. Rev. E74 (2006).

[**15**] P. Saulson, *Thermal Noise in Mechanical Experiments*, Phys. Rev. D (1990).

[**16**] R. Richardson & E. Smith, *Experimental Techniques in Condensed Matter Physics at Low Temperatures*, Key-Westview ABP (1998).

[**17**] F. Pobell, *Matter and Methods at Low Temperatures*, Springer (2007).

[**18**] H. Miyake, *Vibration Isolation System for Fundamental Physics Experiments*, (2006).

[**19**] R. Simmonds, *Josephson Weak Links and Quantum Interference in Superfluid 3-He*, thesis (2002).

[**20**] J. Hoffmann, *Superfluid 4-He: On* $\sin\phi$ *Josephson Weak Links and Dissipation of Third Sound*, thesis (2005).

[**21**] J. Clarke & A. Braginski, *The SQUID Handbook*, WILEY-VCH (2004).

[**22**] B. Hunt et al., *Evidence for a Superglass State in Solid 4He*, Science Vol 324 (2009).

[**23**] B. Hunt, *Relaxation Dynamics of Solid Helium-4*, thesis (2009).